Robust Landing Guidance Law for Impaired Aircraft

P. K. Menon[1], S. S. Vaddi[2], P. Sengupta[3]
Optimal Synthesis Inc, Los Altos, CA, 94022

A guidance law for landing an impaired aircraft is described. The approach involves a planning phase wherein the performance limits of the aircraft are used to design the landing pattern and the reference speed, followed by the guidance computations for generating attitude commands. Commanded attitude can be displayed the pilot on a heads-up display for manual control, or can be coupled to the autopilot. In addition to the attitude commands, the guidance system can also generate the flap deployment schedules, and auto-brake system initiation trigger in equipped aircraft. Guidance system development is based on a point-mass nonlinear model of the aircraft. Feedback linearization technique is used to transform the system dynamics into a linear, time-invariant form. Finite interval differential game formulation is then used to derive the robust optimal guidance law. Inverse transformation of the guidance commands to the original coordinate system produces the roll, pitch and yaw attitude commands. Attitude commands can be tailored for both the crabbed or sideslip flight modes, and for the transitions between them. Simulation results are given to demonstrate the performance of the proposed approach.

I. Introduction

Recently, there has been significant interest at NASA and other aviation research centers in making aircraft resilient with respect to performance impairment. Operational experience in the major wars in the 20th century, civil air transportation and military flight operations over the past three decades have repeatedly demonstrated the capacity of fixed-wing aircraft to survive substantial impairment and continue on to safe landing[1 - 3]. In most cases, pilot skill has been the key factor in ensuring favorable outcomes. Inspired by such examples, researchers at NASA and other aerospace organizations have been investing resources in developing flight control systems that will allow impaired aircraft to land successfully. Eventually, these impairment-adaptive flight control systems are expected to help compensate for the variations in the human pilot skill level, and contribute towards higher levels of flight safety.

Landing is considered to be one of the most hazardous phases of an aircraft flight. Even under normal conditions, landing is the highest-workload phase of flight operations. During this phase, the pilot is required to reduce the aircraft speed while descending, deploy flaps, extend landing gear, align the flight path with the runway centerline, and execute the flare or the roundout[4] maneuver. If crosswinds are present, an additional decrab maneuver will have to be executed at touchdown. Aircraft impairment adds another dimension to this already complex task. By introducing additional uncertainties in the flight envelope, aircraft performance impairment requires the pilot to modify the standard landing procedures under limited information. For instance, flap deployment may have to be delayed or altogether eliminated and the flare maneuver may have to be steeper than nominal to accommodate for the loss of lift. Moreover, impaired aircraft may not have the option of going-around for another landing attempt in case the first attempt fails.

For the present research, it is assumed that inner-loop adaptive stabilization systems such as those described in References 1 and 2 will ensure that the airframe is returned to a stable flying condition after the impairment. Moreover, it will be assumed that the aircraft flight envelope and maneuver limits can be estimated within a certain error bound using algorithms such as those described in Reference 5. The estimated performance models can then be used as the basis for deriving the guidance laws for flare and touchdown. Impairments considered in this paper include the loss of lift from major flying surfaces such as wings and the vertical fin, and partial loss of engine power, including thrust asymmetry.

---

[1] Chief Scientist, 95 First Street, Suite 240, Fellow AIAA.
[2] Research Scientist, 95 First Street, Suite 240, Member AIAA.
[3] Research Scientist, 95 First Street, Suite 240, Senior Member AIAA.

Typical landing sequence of an aircraft is illustrated in Figure 1. The major phases of the landing sequences are indicated by yellow waypoints. Aircraft generally approach the landing area in the downwind direction, with an airspeed of about 20 knots above the reference speed V_{REF} [4, 6], at an altitude of 1500 feet. Note that V_{REF} is 30% higher than the stall speed V_{SO}. This portion of the landing pattern is generally termed as the downwind leg. The flap deployment is initiated when the aircraft is abeam with the runway, at approximately its midpoint. The landing gear is deployed when the aircraft is abeam with the expected touchdown point, indicated by a red star in Figure 1. Flap deployment is complete as the aircraft turns into the Base leg, beginning at waypoint A. The airspeed in the Base leg is about is about 10 knots above V_{REF}. The Final leg of the landing pattern begins when the flight path is aligned with the runway centerline, denoted by the waypoint B in the figure. The dimensions of the approach pattern depend on aircraft performance capabilities. For instance, the turn to base portion of the approach pattern may be about a mile or less for a small general aviation aircraft, but may involve several miles of airspace for a heavy jet aircraft.

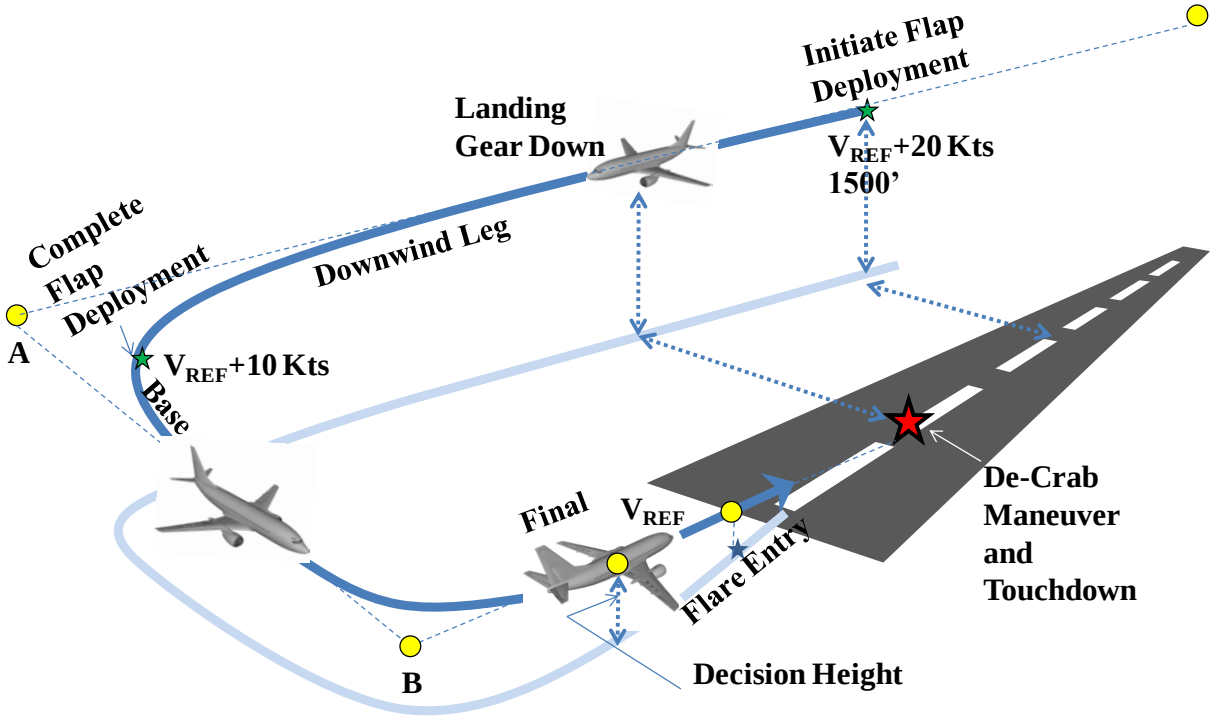

Figure 1. Typical landing Sequence of an aircraft

During the Final leg of the landing pattern, the aircraft flight path is stabilized along the glideslope terminating at a desired aim-point on the runway, and its velocity vector is aligned along the runway centerline, at about 5 knots above V_{REF}. Note that in some cases, the airspace may allow *straight-in* landing trajectory. In that case, the Downwind and Base legs will be absent in the pattern, being replaced by a long Final leg. The aircraft trajectory must be stabilized by the time it reaches 500 feet altitude, otherwise it is recommended that a go-around maneuver is initiated for another landing attempt. Assuming that the trajectory is stabilized, the aircraft can initiate flare maneuver at about 50 feet altitude over the runway threshold, to touchdown at about 1000 feet down the runway. The flare maneuver decreases the aircraft descent rate to between 100 to 200 feet per minute.

The first phase of the landing guidance law is to determine the dimensions of the approach pattern based on a knowledge of the aircraft performance capabilities such as turn rate and stall speed. While these are known under normal conditions, methods such as discussed in Reference 5 must be employed in the case of aircraft impairment. The problem of designing the approach pattern onboard an impaired aircraft will not be further elaborated in the present paper.

All through the Final, the aircraft flight path is required to be aligned along the runway centerline. If the crosswinds are minimal, the trajectory can be aligned without difficulty. However, if crosswinds are present, the aircraft must adopt either a crabbed approach path or a sideslip approach path to continue tracking the runway

centerline[4]. Pilots of large aircraft tend to prefer the crabbed approach since it preserves the visual reference with respect to the horizon until the aircraft is close to the runway surface. Note that this maneuver requires the use of rudder to maintain the sideslip, while applying the ailerons to counter the roll

Very close to the touchdown point, a decrabbing maneuver is executed by rolling the aircraft to touchdown on one of the main gears, while yawing the aircraft nose to align with the runway centerline, and completing the touchdown with the other main gear. The decrab maneuver is carried out simultaneously with the flare. Since both of these maneuvers involve large attitude gyrations close to the ground, extreme care must be exercised to ensure that the airframe does not contact the ground at any point other than at the landing gear. Several example videos illustrating the difficulty of landing in severe crosswinds are available on the worldwide web[7]. While the flare maneuver can be challenging even under ideal conditions, the decrab maneuver during the touchdown in crosswinds adds to the complexity of the task, sometimes requiring a go-around in severe crosswind situations.

The complexity of the flare and decrab maneuvers are largely due to the need to simultaneously satisfy multiple requirements on the flight control system along the path and at the final touchdown point. For instance, the angle of attack has to be precisely controlled so as to ensure a small negative vertical velocity at touchdown to prevent ballooning and bouncing. The forward speed has to be maintained to ensure that sufficient lift is available until wheels touchdown, then rapidly decreased to minimize floating caused by the ground effect. The crab angle must be maintained to align the aircraft velocity vector along the runway centerline until close to the ground, at which time the aircraft must be rolled to ensure that only one of the main landing gears touches the runway surface before the aircraft nose is aligned along the runway centerline. Immediately after this has occurred, the aircraft must be gently rolled back to allow the other landing gear to touchdown, while simultaneously yawing to align the aircraft nose with the runway centerline. If it appears that any of these actions may not lead to a successful landing, the aircraft must immediately execute the go-around procedure by increasing the thrust to takeoff setting, retracting the flaps and the landing gear during the climb out.

On the other hand, if the main gears have touched-down with the nose pointing in the right direction, the aircraft nose must be maintained high enough to rapidly bleed-off the airspeed to allow the nose gear to touchdown. Reverse thrust and spoilers can then be applied to bring the speed down to a point where the aircraft wheel brakes can be safely applied, completing the landing maneuver. While several books on flight control system design discuss the flare control problem[8, 9], none of them have addressed the simultaneous execution of flare and decrab maneuvers in the presence of uncertainties. Interestingly, the complexities of the flare maneuver motivated one of the early attempts in employing neural networks[10] for designing an adaptive control law for this maneuver.

II. Aircraft Models

Although rigid-body dynamics of the aircraft model is often used for autopilot design, point-mass models are more appropriate for use in guidance law development due to their close connection with aircraft performance parameters. The following subsections will discuss two models used in the present work. The first model is used for guidance law derivation, while the second model is used for simulation evaluation of the guidance law.

A. Point-Mass Dynamics

The point-mass model is defined with respect to a runway-fixed coordinate system given in Figure 2. The equations of motion with the assumption of thrust acting along the velocity vector are:

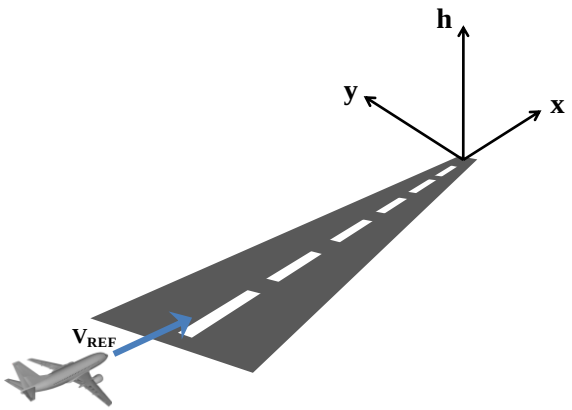

Figure 2. Coordinate System for Point Mass Model

$$\dot{x} = V \cos\gamma \cos\chi \tag{1}$$

$$\dot{y} = V \cos\gamma \sin\chi \tag{2}$$

$$\dot{h} = V \sin\gamma \tag{3}$$

$$\dot{V} = \frac{T - D}{m} - g \sin\gamma \tag{4}$$

$$\dot{\gamma} = \frac{g}{V}\left(\frac{L_h}{W} - \cos\gamma\right) \tag{5}$$

$$\dot{\chi} = \frac{L_y}{mV \cos\gamma} \tag{6}$$

In these equations, T is the thrust, m the mass, V the speed, γ is the flight path angle, χ is the heading angle, L_h and L_y are the aerodynamic forces normal to the velocity vector, and D is the aerodynamic drag. The point-mass model is derived with the assumption that the aircraft is continuously maintained in moment equilibrium using the control surfaces. Thus, the vehicle attitude dynamics is treated as algebraic, and the attitudes are considered to be the control variables.

Note that the forces L_h and L_y can be expressed in terms of lift and the bank angle in bank-to-turn (zero-slip) maneuvers, or in terms of lift and side force for skid-to-turn maneuvers. The lift and side-force components can be expressed in terms of angle of attack and angle of sideslip. Given the orientation of the velocity vector in the inertial frame through the flight path angle γ and the heading angle χ, the pitch-yaw-roll body attitudes necessary to generate a desired angle of attack and the angle of sideslip can be computed. These angles can be used for either pilot guidance, or can be directly coupled to the attitude tracking autopilot.

B. Simulation Model

In addition to the point mass dynamics, the simulation model captures the autopilot-attitude dynamics through linear second-order dynamic systems defined along each axis. Note that this representation of the attitude tracking autopilot dynamics will be exact if its design were based on the feedback linearization methodology. The point-mass equations of motion of the aircraft in an earth-fixed inertial frame are given by:

$$\begin{bmatrix} m\ddot{X} \\ m\ddot{Y} \\ m\ddot{Z} \end{bmatrix} = \begin{bmatrix} c_\theta c_\psi & s_\phi s_\theta c_\psi - c_\phi s_\psi & c_\phi s_\theta c_\psi + s_\phi s_\psi \\ c_\theta s_\psi & s_\phi s_\theta s_\psi + c_\phi c_\psi & c_\phi s_\theta s_\psi - s_\phi c_\psi \\ -s_\theta & s_\phi c_\theta & c_\phi c_\theta \end{bmatrix} \begin{bmatrix} T - \frac{1}{2}\rho V^2 S_{ref} C_x(\alpha,\beta) \\ \frac{1}{2}\rho V^2 S_{ref} C_y(\alpha,\beta) \\ \frac{1}{2}\rho V^2 S_{ref} C_z(\alpha,\beta) \end{bmatrix} + \begin{bmatrix} 0 \\ 0 \\ mg \end{bmatrix} \tag{7}$$

Note that the sine and cosine functions in the transformation matrix in Equation (7) have been abbreviated for the sake of compactness. The control variables in this model are the aircraft attitude components acting through the angle of attack-angle of sideslip variables, and thrust. The autopilot is modeled as three decoupled second order dynamic systems and the engine dynamics is modeled as a first order system, given by following equations:

$$\begin{aligned} \ddot{\phi} &= -k_{p1}(\phi - \phi_{command}) - k_{v1}\dot{\phi} \\ \ddot{\theta} &= -k_{p2}(\theta - \theta_{command}) - k_{v2}\dot{\theta} \\ \ddot{\psi} &= -k_{p3}(\psi - \psi_{command}) - k_{v3}\dot{\psi} \end{aligned} \tag{8}$$

$$\dot{T} = -k_{pT}(T - T_{command}) \tag{9}$$

The variable ρ is the atmospheric density, C_x, C_y, C_z are the body-axis referenced aerodynamic force coefficients, S_{ref} is the reference area, ψ, θ, ϕ are the body attitudes, and T is the thrust. The subscript *command* denotes commanded values. The approximate proportional gains in the autopilot control loops are k_{p1}, k_{p2}, k_{p3} and the derivative gains are denoted by k_{v1}, k_{v2}, k_{v3}. The engine time constant is denoted by k_p.

III. The Landing Guidance Law

Since the point-mass model is nonlinear, it is not readily amenable to the derivation of guidance laws using optimal control[11] and the theory of Differential Games[12]. However, following previous research efforts[13 - 16] the system dynamics can be first transformed into linear, time-invariant form using feedback linearization[17 - 19]. The guidance problem can then be solved using the transformed dynamics, and inverse transformed in terms of the original variables. The resulting solution will be in nonlinear feedback form, suitable for real-time implementation as outlined in the following sections.

C. Feedback Linearization of the Aircraft Point-Mass Dynamics

The first step in the transformation involves the differentiation of the kinematic equations (1) – (3), followed by the substitutions from Equations (4) - (6) to yield:

$$\ddot{x} = \frac{(T - D)}{m}\cos\gamma\cos\chi - \frac{L_h \sin\gamma\cos\chi}{m} - \frac{L_y \sin\chi}{m} \tag{10}$$

$$\ddot{y} = \frac{(T - D)}{m}\cos\gamma\sin\chi - \frac{L_h \sin\gamma\sin\chi}{m} + \frac{L_y \cos\chi}{m} \tag{11}$$

$$\ddot{h} = \frac{(T - D)}{m}\sin\gamma + \frac{L_h \cos\gamma}{m} - g \tag{12}$$

Expressions (10) through (12) describe the aircraft point-mass dynamics in the inertial frame. The transcendental functions given in terms of the flight path angle and the heading angle on the right hand sides of these equations can be computed from the inertial velocity components as:

$$\sin\gamma = \frac{\dot{h}}{\sqrt{\dot{h}^2 + \dot{x}^2 + \dot{y}^2}} \qquad \cos\gamma = \pm\frac{\sqrt{\dot{x}^2 + \dot{y}^2}}{\sqrt{\dot{h}^2 + \dot{x}^2 + \dot{y}^2}} \tag{13}$$

$$\sin\chi = \frac{\dot{y}}{\sqrt{\dot{x}^2 + \dot{y}^2}} \qquad \cos\chi = \frac{\dot{x}}{\sqrt{\dot{x}^2 + \dot{y}^2}} \tag{14}$$

Since the aerodynamic forces on the aircraft are based on its relative speed with respect to the atmosphere, the transformation of the horizontal and vertical lift components to the aircraft attitudes have to be carried out with respect to relative velocity vector. For this purpose, the components of the wind velocity vector are assumed to be specified in the same X-Y-H coordinate system as the equations of motion. The airspeed is then given by:

$$V_a = \sqrt{(\dot{x} - \dot{x}_w)^2 + (\dot{y} - \dot{y}_w)^2 + (\dot{h} - \dot{h}_w)^2} \tag{15}$$

The flight path angle and the heading angle of the airspeed vector can be computed as:

$$\begin{aligned} \sin \gamma_w &= \frac{\dot{h} - \dot{h}_w}{\sqrt{(\dot{x} - \dot{x}_w)^2 + (\dot{y} - \dot{y}_w)^2 + (\dot{h} - \dot{h}_w)^2}} \\ \cos \gamma_w &= \pm \frac{\sqrt{(\dot{x} - \dot{x}_w)^2 + (\dot{y} - \dot{y}_w)^2}}{\sqrt{(\dot{x} - \dot{x}_w)^2 + (\dot{y} - \dot{y}_w)^2 + (\dot{h} - \dot{h}_w)^2}} \end{aligned} \tag{16}$$

$$\begin{aligned} \sin \chi_w &= \frac{\dot{y} - \dot{y}_w}{\sqrt{(\dot{x} - \dot{x}_w)^2 + (\dot{y} - \dot{y}_w)^2}} \\ \cos \chi_w &= \frac{\dot{x} - \dot{x}_w}{\sqrt{(\dot{x} - \dot{x}_w)^2 + (\dot{y} - \dot{y}_w)^2}} \end{aligned} \tag{17}$$

The equations of motion can then be recast in terms of atmosphere-relative velocity vector to yield:

$$\ddot{x} = \frac{(T - D)}{m} \cos \gamma_w \cos \chi_w - \frac{L_{hw} \sin \gamma_w \cos \chi_w}{m} - \frac{L_{yh} \sin \chi_w}{m} = U_x \tag{18}$$

$$\ddot{y} = \frac{(T - D)}{m} \cos \gamma_w \sin \chi_w - \frac{L_{hw} \sin \gamma_w \sin \chi_w}{m} + \frac{L_{yw} \cos \chi_w}{m} = U_y \tag{19}$$

$$\ddot{h} = \frac{(T - D)}{m} \sin \gamma_w + \frac{L_{hw} \cos \gamma_w}{m} - g = U_h \tag{20}$$

The right hand sides of Equations (18) - (20) are next denoted by pseudo-control variables U_x, U_y, U_z to define the transformed dynamics of the aircraft. Note that the system is in linear, time-invariant and decoupled form in terms of the pseudo-control variables. The state variables in the transformed model are the position and velocity components of the aircraft in the inertial frame. The pseudo-control variables are the acceleration components in the inertial frame.

The pseudo-control variables can be inverse transformed to thrust, pitch, yaw, and roll attitude using algebraic transformations, as will be illustrated in Section E. An available degree of freedom in this transformation is the fact that the aircraft can be operated in bank-to-turn or skid-to-turn modes. Pitch-yaw attitudes at arbitrary roll attitudes can be used to create skid-to-turn maneuvers such as the crabbed approach, while pitch-yaw -roll attitudes can be used to create bank-to-turn maneuvers useful for sideslip approaches.

It is reasonable to assume that minor changes to aircraft thrust will be made by the auto-throttle or the pilot to keep the speed essentially constant during the descent. Consequently, the thrust magnitude can be assumed to be equal to drag.

Since the transformed point-mass dynamics is linear and time invariant with respect to the control variables, linear optimal control and differential game theories can be directly applied to this guidance problem, as will be illustrated in the following section.

D. Robust Finite Interval Optimal Guidance

Since the transformed point-mass dynamics of the aircraft form is in decoupled form, the guidance law derivation will only be illustrated along one the vertical direction. The development for the lateral direction can be carried out in an entirely analogous form.

The feedback linearized model of the aircraft In the vertical direction can be written as:

$$\ddot{Z} = a - b \tag{21}$$

Here a is acceleration in the vertical direction and b represents the external disturbance in the same direction. A similar equation can be written for the Y coordinate as well. The objective of the landing guidance law is to transfer the aircraft from its initial position and velocity to a desired waypoint with a specified velocity at a specified final time, while subjecting it to least amount of acceleration. The guidance law should simultaneously minimize the impact of external disturbances on the trajectories. This can be achieved by minimizing a performance index of the form:

$$J = \left[\frac{1}{2}S_1\left(Z_f - Z_{fdes}\right)^2 + \frac{1}{2}S_2\left(\dot{Z}_f - \dot{Z}_{fdes}\right)^2\right]\Bigg|_{t=t_f} + \frac{1}{2}\int_0^{t_f}\left(Ra^2 - \varepsilon b^2\right)dt \tag{22}$$

The first term in the performance index penalizes the deviations in the aircraft position from a specified waypoint location at the specified final time and the second term penalizes the velocity error. The first term in the integrand imposes the objective of minimizing the acceleration. The second term in the integrand arises from the need to make the guidance law robust with respect to external disturbance b. The negative sign of this term arises from the Differential Game view of the disturbances, which assumes that the disturbances always act in such a way as to maximize the performance index,

The parameters S_1, S_2 and R can be chosen to establish relative weighting between the terminal position error, velocity error and the acceleration magnitudes. The variational Hamiltonian for the optimal control problem (21), (22) can be used to derive the co-state equations while enforcing the optimality condition. This process yields:

$$H = \frac{1}{2}\left(Ra^2 - \varepsilon b^2\right) + \lambda_1\dot{Z} + \lambda_2(a - b) \tag{23}$$

$$\dot{\lambda}_1 = 0 \qquad \lambda_1 = \lambda_1(0) \tag{24}$$

$$\dot{\lambda}_2 = -\lambda_1 \qquad \lambda_2 = \lambda_2(0) - \lambda_1(0)t \tag{25}$$

Optimality condition[11] can be used to derive the optimal control and worst case disturbance as:

$$a = -\frac{\lambda_2}{R} = -\frac{\left(\lambda_2(0) - \lambda_1(0)t\right)}{R} \tag{26}$$

$$b = -\frac{\lambda_2}{\varepsilon} = -\frac{\left(\lambda_2(0) - \lambda_1(0)t\right)}{\varepsilon} \tag{27}$$

Boundary conditions on the co-states at the specified final time are given by:

$$\lambda_{1f} = S_1\left(Z_f - Z_{fdes}\right) \tag{28}$$

$$\lambda_{2f} = S_2\left(\dot{Z}_f - \dot{Z}_{fdes}\right) \tag{29}$$

Substituting the expression for control and worst case disturbance into the transformed equations of motion and integrating yields the following expressions for acceleration, velocity and position:

$$\ddot{Z} = -\frac{\left(\lambda_2(0) - \lambda_1(0)t\right)}{R} + \frac{\left(\lambda_2(0) - \lambda_1(0)t\right)}{\varepsilon} = -\left(\lambda_2(0) - \lambda_1(0)t\right)\left(\frac{1}{R} - \frac{1}{\varepsilon}\right) \tag{30}$$

$$Z_f = Z(0) + \dot{Z}(0)t_f - \left(\frac{1}{R} - \frac{1}{\varepsilon}\right)\frac{\lambda_2(0)t_f^2}{2} + \left(\frac{1}{R} - \frac{1}{\varepsilon}\right)\frac{\lambda_1(0)t_f^3}{6} \tag{31}$$

$$\dot{Z}_f = \dot{Z}(0) - \lambda_2(0)t_f\left(\frac{1}{R} - \frac{1}{\varepsilon}\right) + \lambda_1(0)t_f^2\left(\frac{1}{R} - \frac{1}{\varepsilon}\right) \tag{32}$$

Substituting these expressions in the expressions for co-state boundary conditions (28) and (29) yields the following linear system of equations:

$$\begin{bmatrix}\lambda_1(0)\\ \lambda_2(0)\end{bmatrix} = \frac{1}{Det}\begin{bmatrix} -\left(\frac{1}{R} - \frac{1}{\varepsilon}\right)\frac{S_1 t_f^2}{2} & \left(\frac{1}{R} - \frac{1}{\varepsilon}\right)S_2 t_f + 1 \\ -\left(\frac{1}{R} - \frac{1}{\varepsilon}\right)\frac{S_1 t_f^3}{6} + 1 & \left(\frac{1}{R} - \frac{1}{\varepsilon}\right)\frac{S_2 t_f^2}{2} + t_f \end{bmatrix}\begin{bmatrix} S_2(\dot{Z}_{fdes} - \dot{Z}(0)) \\ S_1(Z_{fdes} - Z(0) - \dot{Z}(0)t_f) \end{bmatrix} \tag{33}$$

with

$$Det = \left[\left(-\left(\frac{1}{R} - \frac{1}{\varepsilon}\right)\frac{S_1 t_f^2}{2}\right)\left(\left(\frac{1}{R} - \frac{1}{\varepsilon}\right)\frac{S_2 t_f^2}{2} + t_f\right) - \left(-\left(\frac{1}{R} - \frac{1}{\varepsilon}\right)\frac{S_1 t_f^3}{6} + 1\right)\left(\left(\frac{1}{R} - \frac{1}{\varepsilon}\right)S_2 t_f + 1\right)\right]$$

Given the waypoint locations and the desired speeds at those waypoints, the expression (33) can be solved to yield the initial values of the co-states. These can then be used to compute the control in the vertical direction at the initial time as:

$$a(0) = -\frac{\lambda_2(0)}{R} \tag{34}$$

Following Reference 11, this control variable can be recast in terms of time-to-go to define the control variable at the initial time given by (34) as the control variable at the present time *t*.

E. Inverse Transformation

The finite-interval guidance law developed in the previous section computes the acceleration components in the vertical and horizontal directions for landing the aircraft in the presence of disturbances, while satisfying waypoint constraints. These acceleration components can be transformed into the body attitude commands for use by the pilot in a heads-up display or for direct tracking by the autopilot. Since this transformation process is complex, it will be carried out in multiple steps in the following.

Given U_y and U_h, the components of the accelerations normal to the relative velocity vector required to execute the landing trajectory, and the assumption that $T=D$, the components of the aerodynamic forces normal to the relative velocity vector can be computed from:

$$L_{yw} = -\frac{1}{\cos\chi_w}\left(mU_y + L_{hw}\sin\gamma_w\sin\chi_w\right) \tag{35}$$

$$L_{hw} = \frac{m}{\cos\gamma_w}\left(U_h + g\right) \tag{36}$$

The next step in the transformation is that of converting the horizontal and vertical forces given by equations (35) and (36) first into aerodynamic coefficients, and then into aircraft attitudes. Note that the transformed model involves only the two components of acceleration with respect to the inertial frame. However, the aircraft attitude has three components, namely, the pitch, yaw and roll attitudes. Thus, the transformation from the acceleration components into attitudes has a free degree of freedom. This additional degree of freedom can be used to enforce an additional constraint.

During conventional three-dimensional maneuvers involving aircraft with a vertical plane of symmetry, this constraint is enforced through the *coordinated flight* requirement, which constrains the angle of sideslip to remain zero throughout maneuvers. A second approach to maneuvering is through the skid-to-turn maneuvers, which explicitly employ an angle of sideslip to generate lateral accelerations. Such maneuvers may occur in impaired aircraft which may not have a vertical plane of symmetry. Skid-to-turn maneuvers may also arise during crabbed flight under crosswind conditions. In fighter aircraft, the skid maneuver is often used for pointing body-fixed weapon systems in a desired direction. Notably, most axisymmetric missiles employ skid-to-turn maneuvers during their normal operation. The following sections will discuss transformations to enable both these maneuvers.

F. Skid-to-Turn Mode

The skid-to-turn mode may be employed during the stabilized approach phase of the landing. In the lateral direction, this mode is characterized by the existence of non-zero angles of sideslip. Pitch and yaw attitudes are used to realize the desired angle of attack and angle of sideslip, with the roll attitude maintained at zero. Firstly, the desired lift and side-force coefficients are computed using the forces given by Equations (35)- (36) to yield:

$$C_{L\_desired} = \frac{L_{hw}}{0.5\rho V_a^2 S} \qquad C_{S\_desired} = \frac{L_{yw}}{0.5\rho V_a^2 S} \tag{37}$$

Angle of attack and angle of sideslip corresponding to the desired lift and side-force coefficients can be determined from the tables listing the relationship between angle of attack and lift coefficient, and angle of sideslip and sideforce. If these tables are symbolically denoted by the functions f_L and f_S, these computations can be summarized as:

$$\alpha_w = f_L^{-1}\left(C_{L\_desired}\right) \qquad \beta_w = f_S^{-1}\left(C_{S\_desired}\right) \tag{38}$$

At small angles of attack and angle of sideslip, these functional relationships are linear. However, they relationships can be highly nonlinear if the aircraft is operating at extreme angle of attack and angle of sideslip. Once the angle of attack and angle of sideslip are computed, the next step in the process is that of computing the corresponding yaw-pitch attitudes or pitch-roll attitudes. For small angles of attack and angle of sideslip, the roll-pitch-yaw attitudes can be expressed as:

$$\phi = 0 \qquad \theta = \alpha_w + \gamma_w \qquad \psi = -\chi_w - \beta_w \tag{39}$$

G. Bank-To-Turn Mode

The bank-to-turn mode is employed under normal aircraft operations. Angle of attack and bank angle are used to realize the desired aerodynamic forces in this mode. Since the angle of sideslip is required to be zero, the side-force coefficients are not used in the computations. The aerodynamic lift and the desired lift coefficient are first computed as:

$$L = \sqrt{L_{hw}^2 + L_{yw}^2} \Rightarrow C_{L\_desired} = \frac{L}{0.5\rho V_a^2 S} \tag{40}$$

Next, the angle of attack and bank angle are computed as:

$$\alpha_{Tw} = f_L^{-1}\left(C_{L\_desired}\right) \qquad \Phi_w = \tan^{-1}\left(\frac{L_{yw}}{L_{hw}}\right) \tag{41}$$

These controls will yield Bank-to-Turn or Coordinated maneuvers ($\beta=0$). Roll-pitch attitudes for small angle of attack and small bank angles can then be recovered as:

$$\phi = -\Phi_w \qquad \theta = \alpha_{Tw} + \gamma_w \tag{42}$$

Note that the expressions for attitude in terms of the angle of attack and bank angle assume small angle approximations. The relationships for large angles are a little more involved.

Although aircraft operate in either one of the modes during most of their flight, there is a specific maneuver which employs a combination of these modes. This is the terminal decrab maneuver, wherein the aircraft nose is intentionally rotated away from the wind direction to point along the runway centerline. This creates an angle of sideslip, requiring the aircraft to bank towards the wind to counter the side force to keep the aircraft aligned along the runway centerline.

IV. Closed Loop Simulation Results

The guidance law discussed in the previous section is evaluated in a simulation. The following parameters extracted from the NASA GTM aircraft model[20] are used in the simulation.

$$m = 198000 \ \ lbs \qquad S_{ref} = 1951 \qquad \rho = 0.0075 \ \ slug \ / \ ft^3 \qquad V_{stall} = 107 \ \ knots \qquad V_{ref} = 145 \ \ knots$$

The following autopilot time-constants from Reference 9 are used in the roll, pitch, and yaw channels:

$$t_{cr} = 6.3s \qquad t_{cp} = 3.88\ s \qquad t_{cy} = 6.3s$$

The damping ratios for all three axes are set as: $\zeta_r = \zeta_p = \zeta_y = 0.707$.

After several trials, the terminal state weighting factors, control weighting factor and the disturbance weighing factor for the optimal guidance law are chosen as:

$$S_1 = 1e2 \qquad S_2 = 1e8 \qquad R = 1 \qquad \varepsilon = 2$$

A. Guidance Law Implementation

Only the Final leg of the landing pattern consisting of stabilized approach, flare and decrab are presented in this paper, since they form the most crucial portions of the landing trajectory. Three waypoints are chosen for the final landing phase based on CFR Part 14[5]. These are: (1) stabilized approach checkpoint (2) threshold and (3) the touchdown point. CFR Part 14 recommends the glideslope to be between 2.5degrees and 3degrees. The glideslope is set to 2.75degrees in the present simulations, with the duration of flare being set to 6 seconds and the vertical speed at touchdown required to be at 200 ft/min. Desired states at the three waypoints are specified as:

$$h_1 = 500 \ \ ft, \quad \dot{h}_1 = V_{ref} \ \sin \ 2.75^0, \quad y_1 = 0, \quad \dot{y}_1 = 0 \quad @ \ x_1 = -\frac{500 \ - 50}{\tan \ 2.75^0} - L_{rwy} \tag{43}$$

$$h_2 = 50 \ \ ft, \quad \dot{h}_2 = V_{ref} \ \sin \ 2.75, \quad y_2 = 0, \quad \dot{y}_2 = 0 \quad @ \ x_2 = -L_{rwy} \tag{44}$$

$$h_3 = 0, \quad \dot{h}_3 = 200 \ \ ft / \min, \quad y_3 = 0, \quad \dot{y}_3 = 0, \quad @ \ x_3 = V_{ref} \ \cos \ 2.75^0 * t_{flare} \ - L_{rwy} \tag{45}$$

These serve as boundary conditions for optimal guidance law in the Final. The time-to-go for the guidance law is computed using the equation:

$$t_{2go} = -\frac{range \ \_ 2 \_ waypo \ \ int}{range \ \_ rate} = -\frac{(x - x_i)^2 + (y - y_i)^2 + (z - z_i)^2}{(x - x_i)\dot{x} + (y - y_i)\dot{y} + (z - z_i)\dot{z}} \tag{46}$$

The aircraft is expected to stay close to the reference speed throughout the Final segment of the landing pattern. Thrust required for maintaining constant airspeed is computed by setting the derivative of the airspeed to zero to yield:

$$0 = \dot{V}_a = \frac{1}{V_a}\begin{bmatrix}(\dot{x} - \dot{x}_w) & (\dot{y} - \dot{y}_w) & (\dot{h} - \dot{h}_w)\end{bmatrix}\begin{bmatrix}U_x \\ U_y \\ U_h\end{bmatrix} \tag{47}$$

Since U_y, U_h are known from the guidance law computations, the value of U_x that will ensure constant airspeed can be computed. This value of acceleration, together with the lateral and vertical aerodynamic forces, and the drag can be used to compute the thrust setting that will achieve constant airspeed. This thrust setting is used until the aircraft reaches the stabilized approach check altitude of 500 feet. The thrust is fixed beyond that point.

B. Landing Under Large Initial Condition Errors

In this landing scenario, the aircraft starts with a lateral error of 500 ft with an initial altitude error of 200 ft from the glideslope at an initial flight path angle of 2.6 degrees. Figure 3 through Figure 5 show the landing trajectories in three dimensions, vertical plane and horizontal plane respectively. It may be observed that the position errors in the lateral and vertical directions are corrected by the time the aircraft reaches the stabilized approach check altitude. Thereafter, the aircraft remains very close to the glideslope in the vertical direction and aligned with the runway centerline in the lateral direction. Figure 6 gives the descent rate of the aircraft. Figure 7 and Figure 8 provide the trajectory in the vertical plane and the descent rate as a function of height above the ground during the flare. Descent rate at touchdown is about 197 ft/min, which is within the specified rate of 100 - 200 ft/min in CFR Part 14.

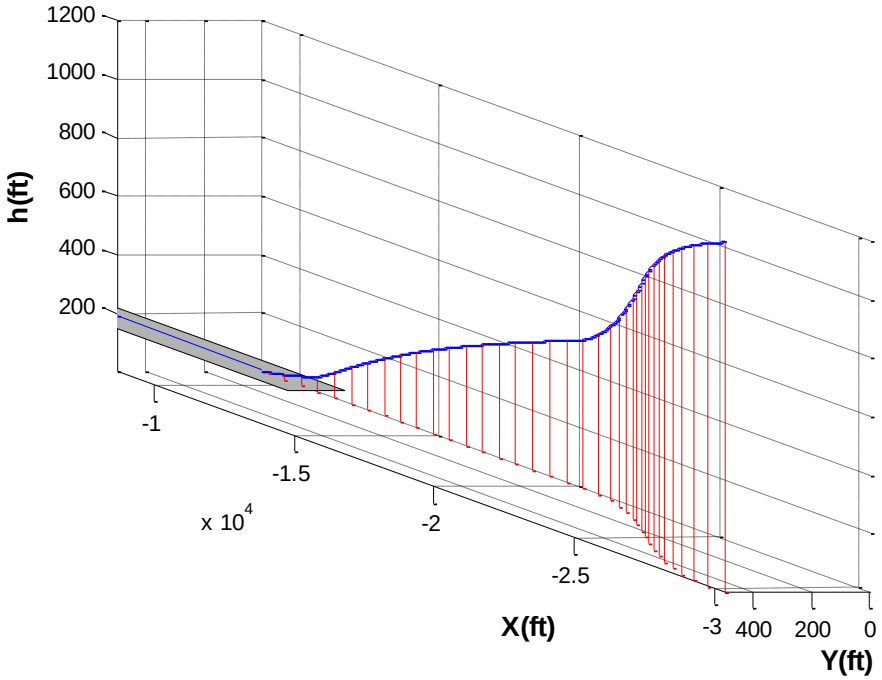

Figure 3. Final segment of the Landing Trajectory in 3-D

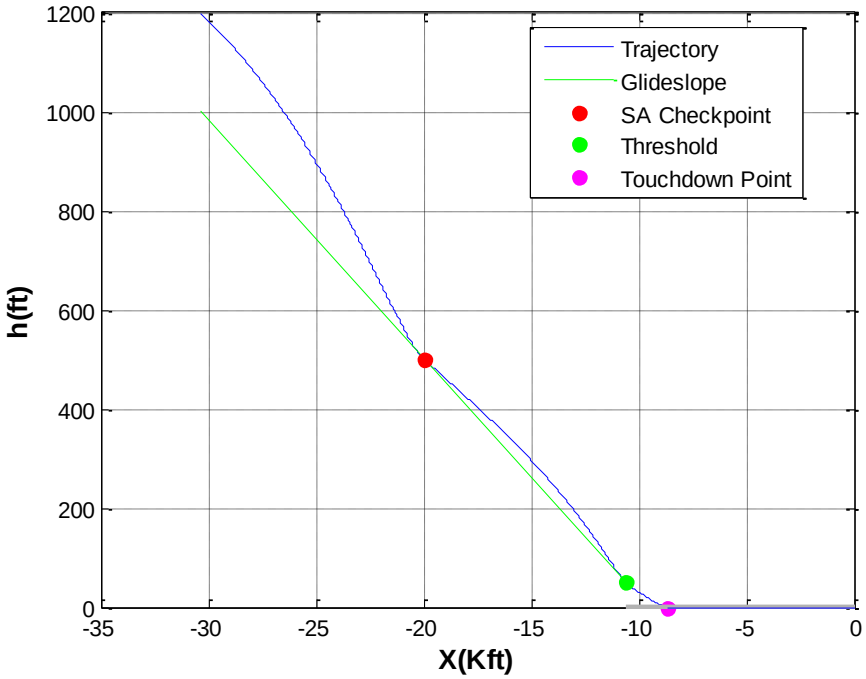

Figure 4. Landing Trajectory in the Vertical Plane

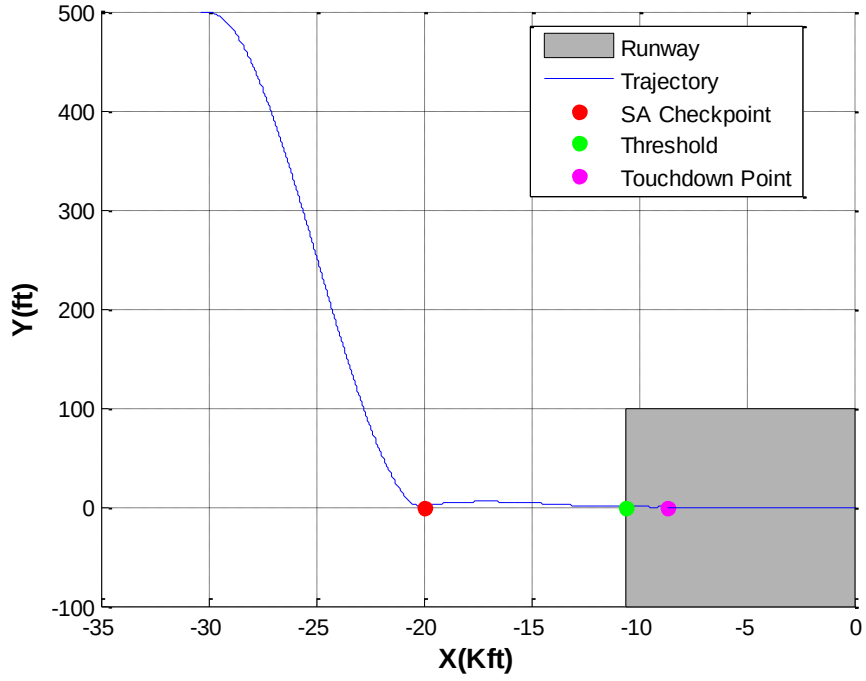

Figure 5. Landing Trajectory in the Horizontal Plane

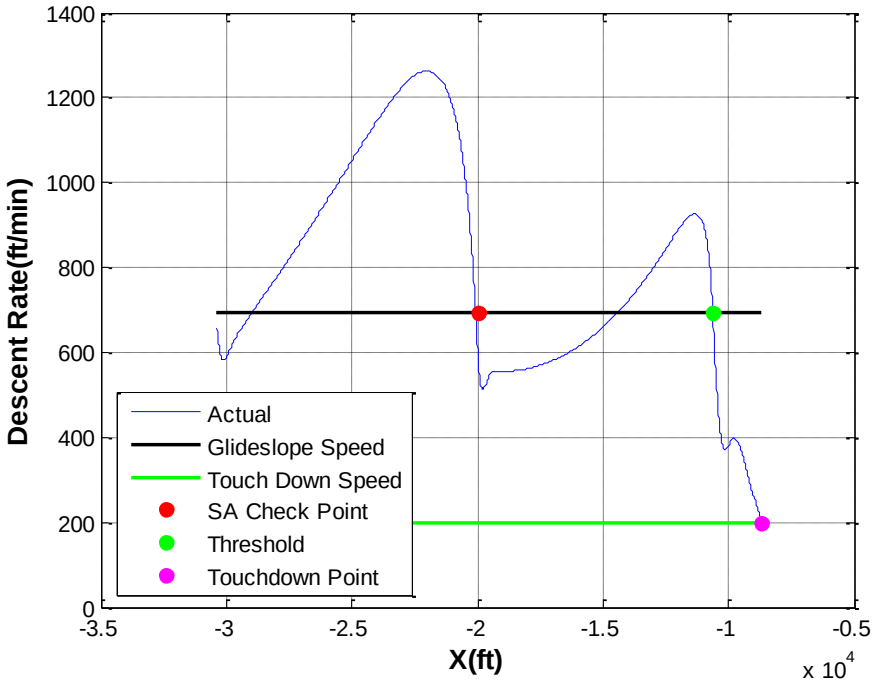

Figure 6. Descent Rates during the Stabilized Approach and Flare

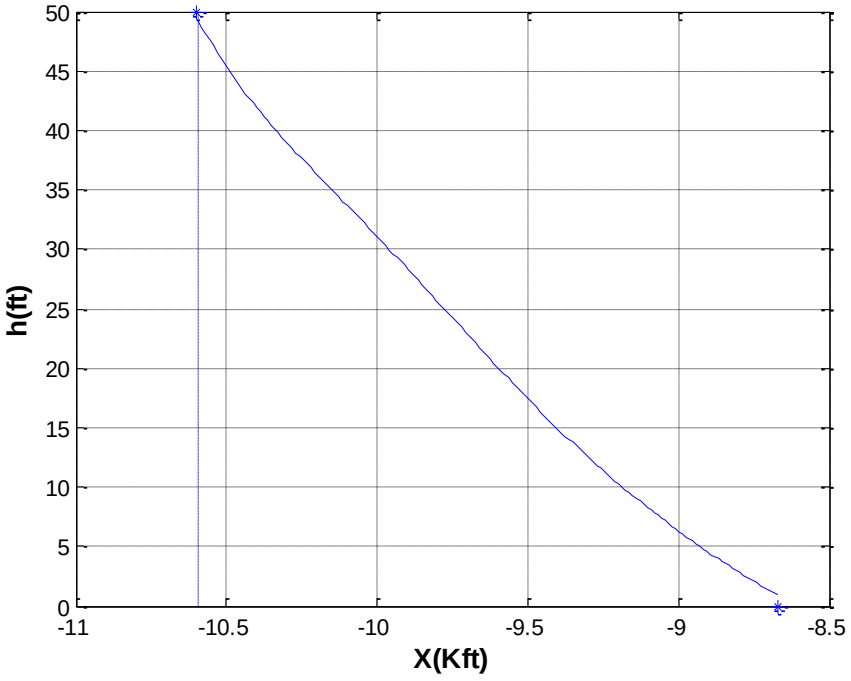

Figure 7. Trajectory in the Vertical Plane during the Flare Maneuver

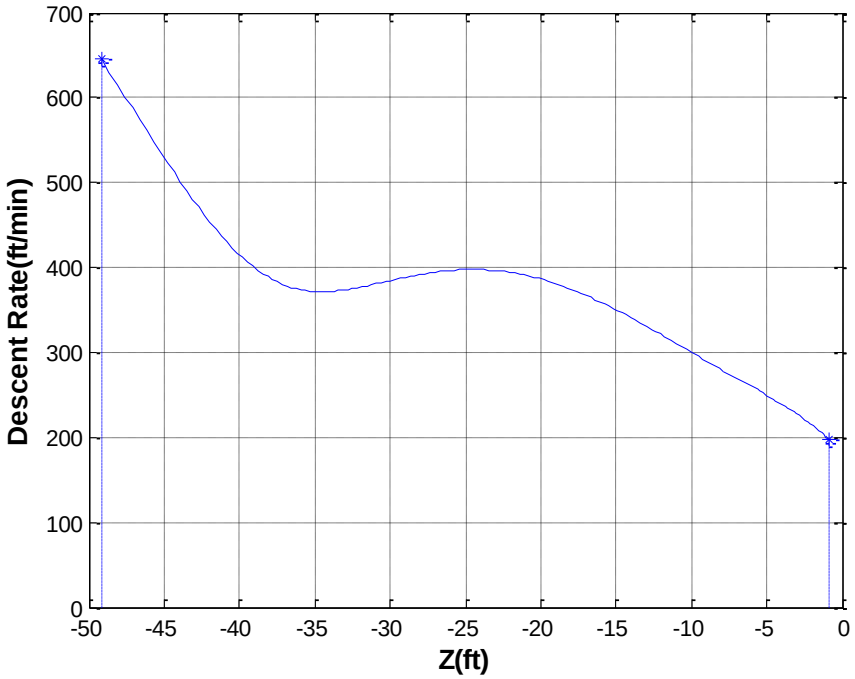

Figure 8. Descent Rate as a function of Altitude above the Runway during the Flare Maneuver

Figure 9 shows that the reference airspeed remained within 3 Knots of the specified value throughout the landing trajectory. The commanded and the actual thrust profiles are shown in Figure 10. The observed thrust transients are due to the tight control tolerances used in the present study. Note that the magnitudes are well within the maximum thrust capacity of 40,000 lbf for the NASA GTM aircraft model.

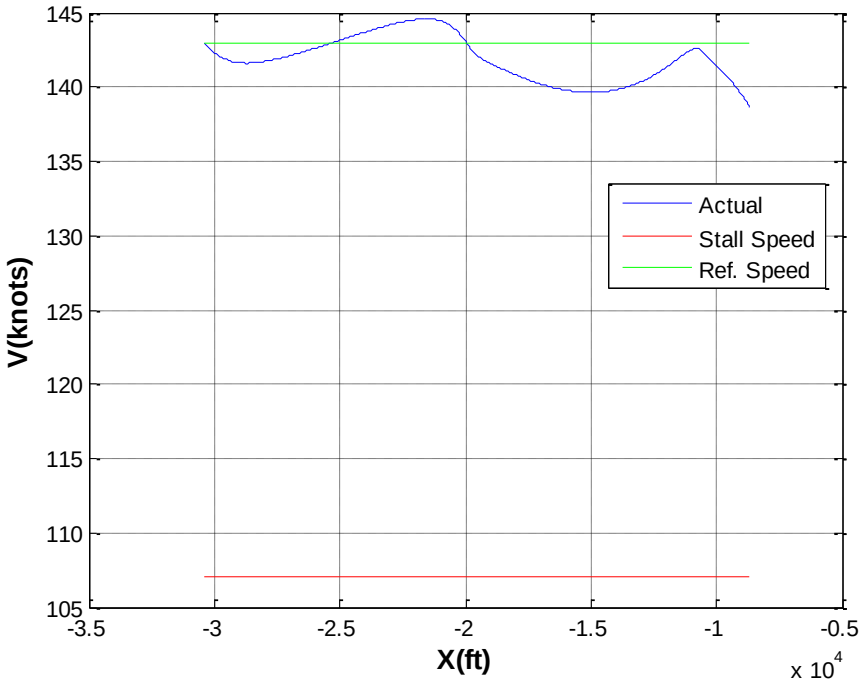

Figure 9. Airspeed

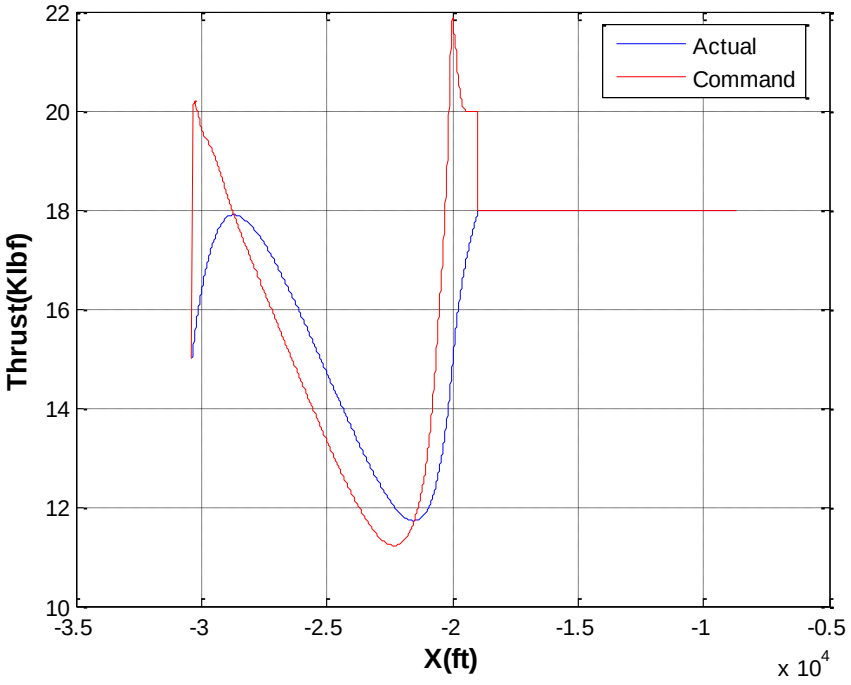

Figure 10. Commanded and Actual Thrust

Figure 11 through Figure 13 give the commanded and the actual roll, pitch and yaw attitudes. Commanded and the actual values of the roll attitude are zero during the stabilized approach phase. Following the current operating procedure of using crabbed approach, the yaw attitude is used to maintain the aircraft on course until the flare maneuver, at which time, the roll angle is used to keep the aircraft aligned along the runway centerline. This can be

observed in Figure 11, which shows minor roll gyrations towards the end. Pitch attitude history given in Figure 12 assumes negative values before the aircraft approaches the stabilized approach check altitude to correct for the 200 ft excess altitude. The pitch control activity remains small after this stage. The aircraft pitches up by 2 degrees to reduce the descent rate during the flare. The yaw attitude history shown in Figure 13 exhibits most activity before the stabilized approach check altitude is reached. Thereafter, the aircraft trajectory remains aligned with the runway centerline with very little yaw control activity. The red lines in all three plots show the attitude commands generated by the guidance law and the blue lines indicate the aircraft attitude. The jumps in commanded values at the waypoints are due to the fact that the control objective changes between each waypoint segment and no requirement has been placed on the smoothness of control. If desired, such a requirement can be imposed by introducing additional dynamics at the input. Studies such as these will be of future interest.

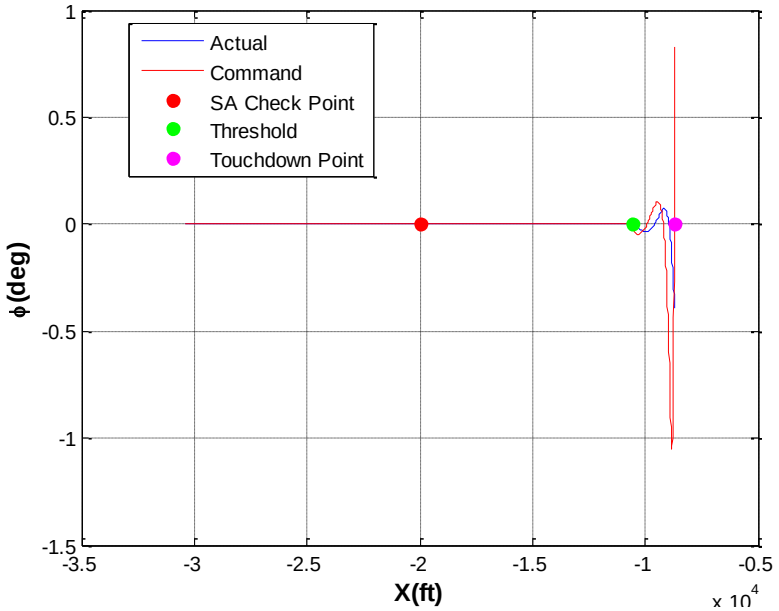

Figure 11. Actual and Commanded Roll Attitude Histories

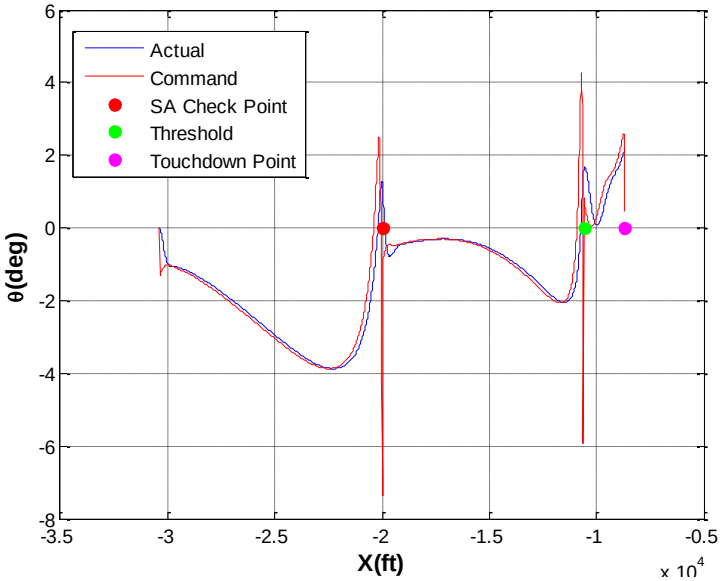

Figure 12. Actual and Commanded Pitch Attitude Histories

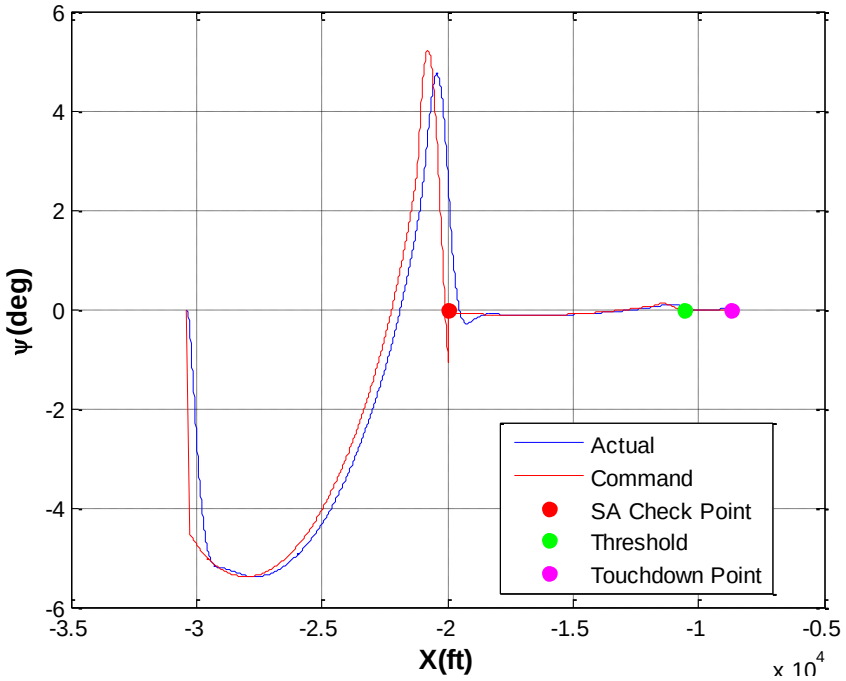

Figure 13. Actual and Commanded Yaw Attitude Histories

C. Landing Under a 20 Knot Crosswind

A 20 knot steady crosswind along the positive Y axis is introduced into the simulation in order to study the response of the guidance law. The landing trajectory in the horizontal plane is given in Figure 14. It can be seen in this figure that the aircraft corrects 500 ft lateral offset in the presence of crosswind by the time it reaches the stabilized approach check altitude. The pronounced bulge in the trajectory between the stabilized approach check point and the threshold is due to the combined effect of the crosswind and the airspeed vector orientation requirement at the waypoint. The specified conditions at the runway threshold and touchdown point are met by the guidance law. The aircraft lands with a yaw attitude less than 0.01degrees, lateral offset of 0.37 ft and heading angle of -1.5 degrees. Descent rate at touchdown is 218ft/min, which is slightly higher than the specified maximum rate, as seen in Figure 15.

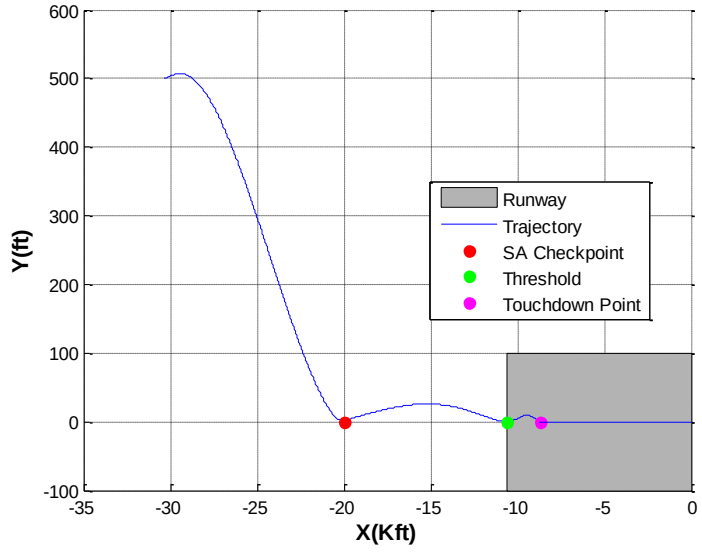

Figure 14. Landing Trajectory in the Horizontal Plane under 20 Knot Crosswind

Figure 16 through Figure 17 provides comparisons of the yaw attitude, roll attitude and angle of sideslip histories under 20 knot crosswind with those of the nominal landing scenario discussed in the foregoing. The yaw attitude of the aircraft under crosswind assumes larger values than the nominal landing scenario. This is more pronounced in the segment between the stabilized approach check altitude and the runway threshold, where the yaw attitude assumes a value of about 8 degrees in order to tighten the lateral deviation between the aircraft trajectory and the runway centerline in the presence of crosswind. However, during the decrab maneuver the yaw attitude jumps back to align the nose of the aircraft with the runway, angle of sideslip develops and the aircraft banks in the direction of the crosswind as can be observed in Figure 18. It should be noted that the aircraft rolls by as much as 10 degrees as opposed to the near zero values in the nominal landing scenario.

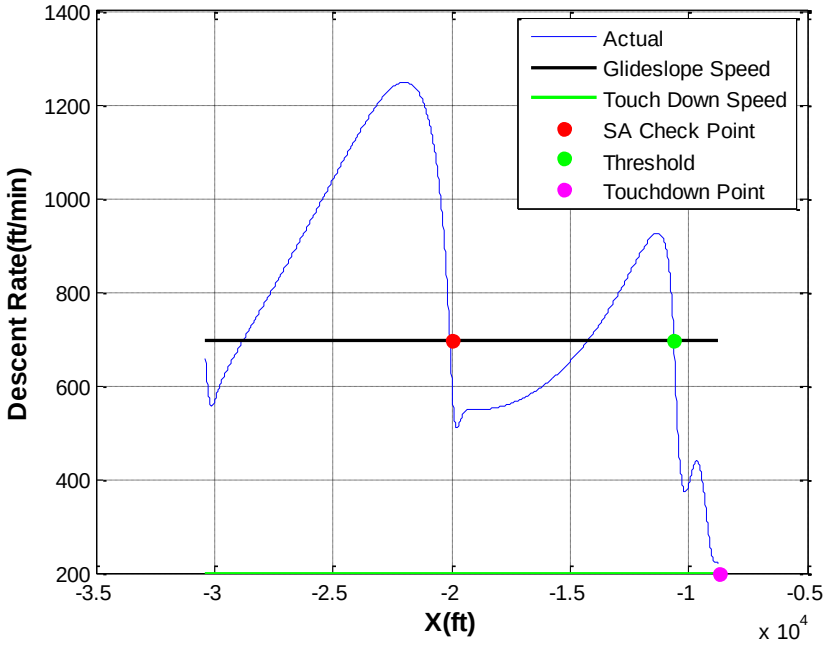

Figure 15. Descent Rate during the Stabilized Approach and Flare under 20 Knot Crosswind

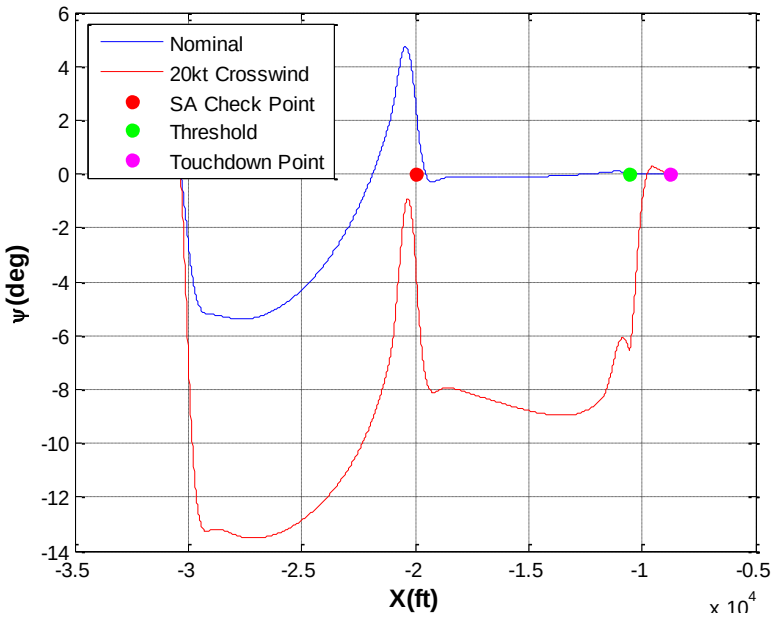

Figure 16. Yaw Attitude History during the Stabilized Approach and Flare

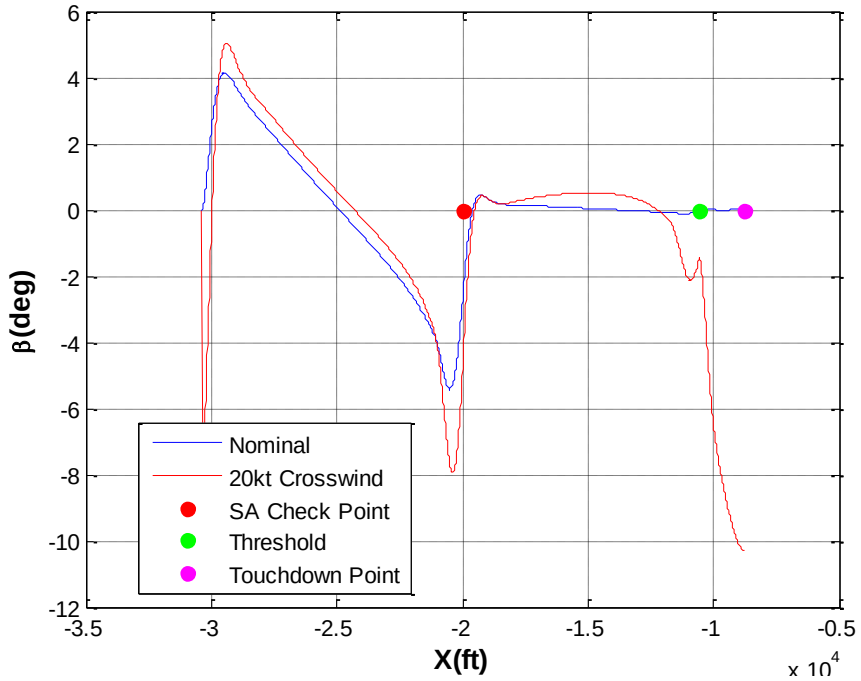

Figure 17. Angle of Sideslip History during the Stabilized Approach and Flare

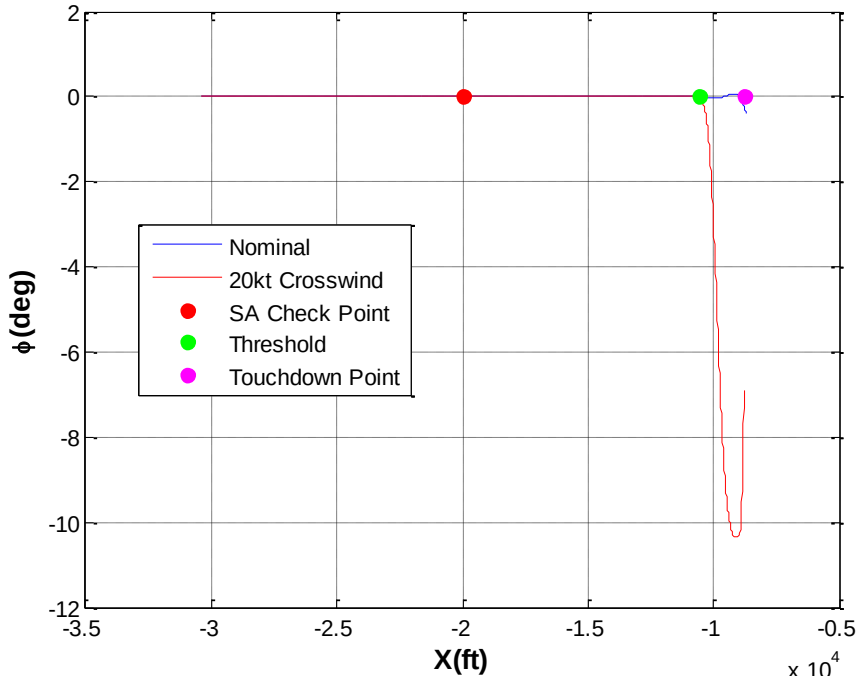

Figure 18. Roll Attitude History during the Stabilized Approach and Flare

D. Landing Under 40% Symmetric Reduction of Lift Coefficient

This scenario simulates the loss of lift due to aircraft impairment. The aircraft lift coefficient is reduced by 40% to simulate this case. The landing at 165 knots, 170knots and 175knots are then investigated. Figure 19 gives the vertical plane trajectories at all three speeds and the nominal trajectory at 142 knots landing speed. All four trajectories are close to each other indicating that the guidance law was able to accommodate for the reduction in the lift coefficient. This is also confirmed by the descent rate plots in Figure 20 where the 40% loss of lift coefficient

result in a vertical speed of about 185 ft/s when compared with the 197ft/s in the nominal scenario. The difference between the two scenarios manifests itself in the angle of attack and pitch attitude histories shown in Figure 21 and Figure 22 respectively. The aircraft under 40% loss of lift coefficient pulls a larger angle of attack and pitch attitude to generate similar lift magnitudes during the flare maneuver. If higher landing speeds are permissible, the maximum angle of attack and pitch attitude will be observed to decrease due to the higher dynamic pressure.

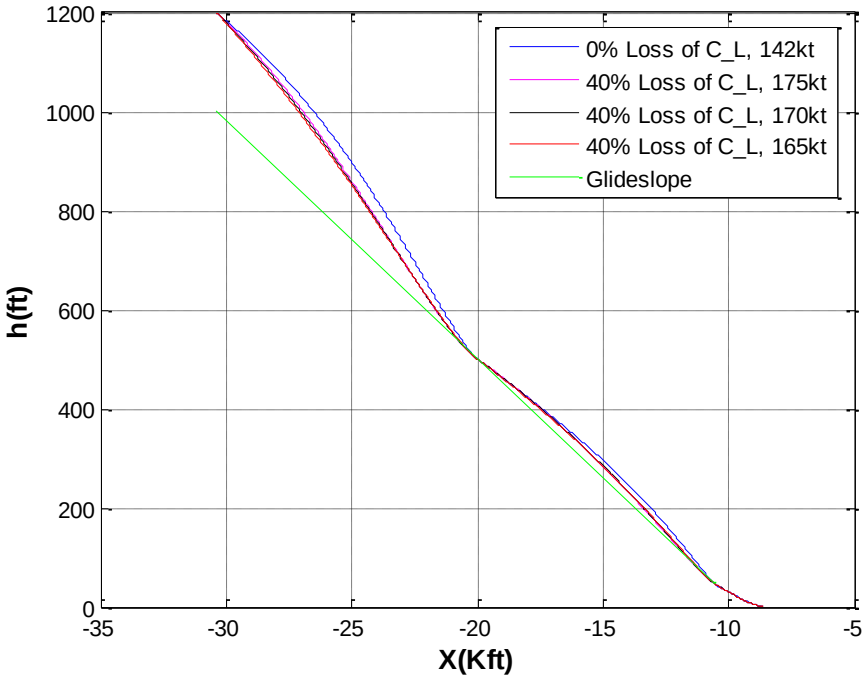

Figure 19. Vertical Plane Trajectories for Different Landing Speeds with 40% Loss of Lift Coefficient

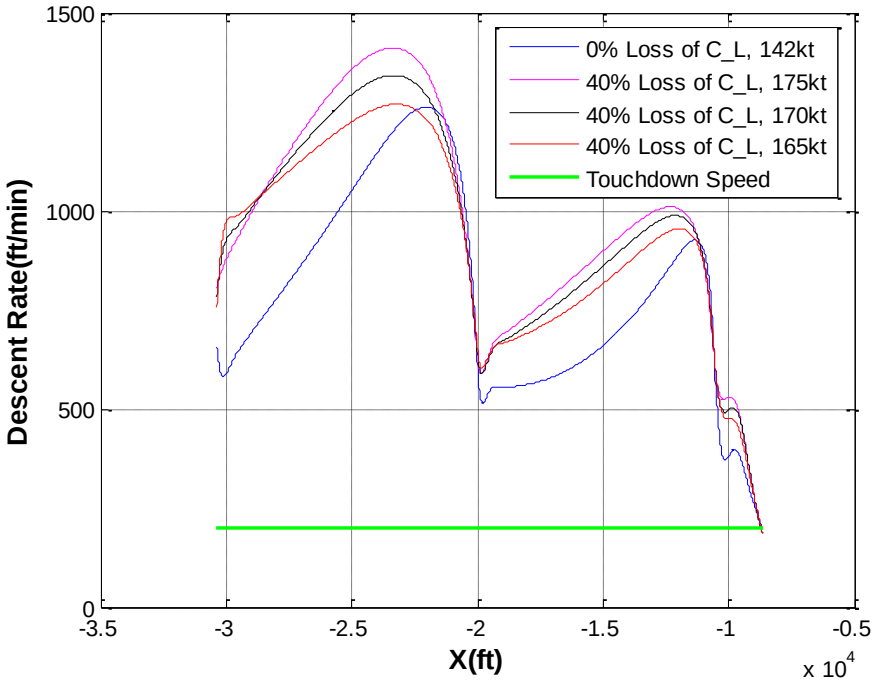

Figure 20. Descent Rate Histories for Different Landing Speeds at 40% Loss of Lift Coefficient

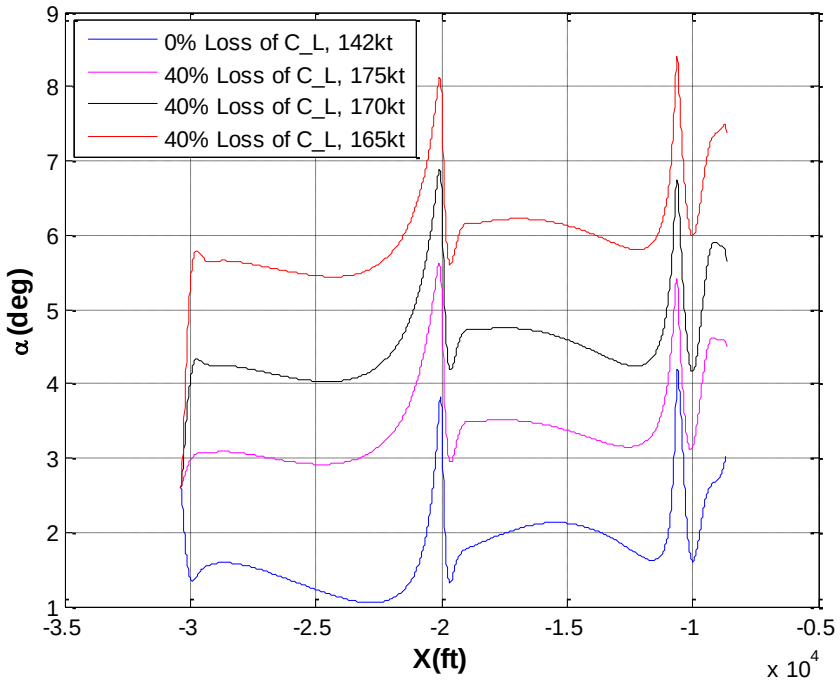

Figure 21. Angle of Attack Histories for Different Landing Speeds at 40% Loss of Lift Coefficient

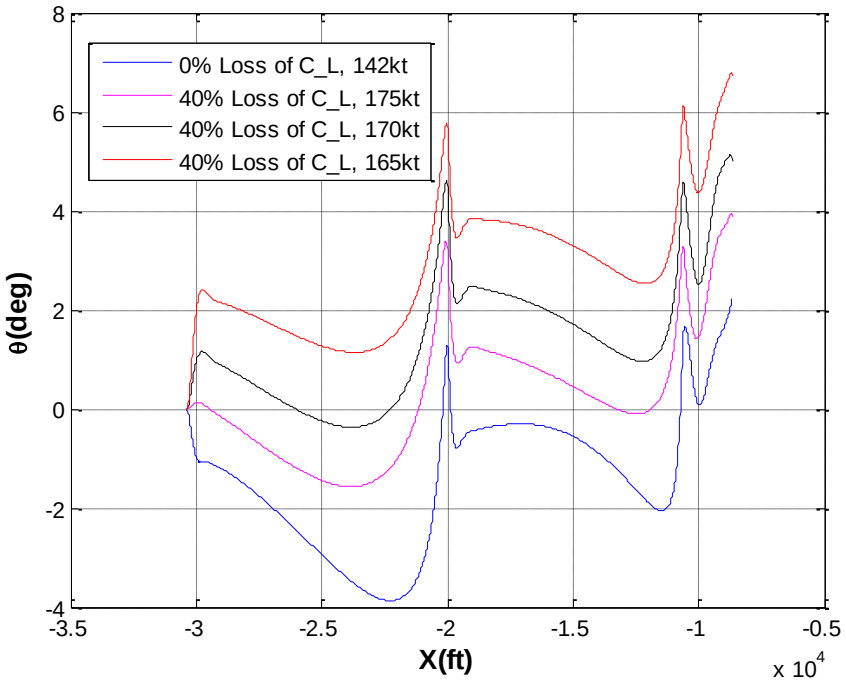

Figure 22. Pitch Attitude Histories for Different Landing Speeds at 40% Loss of Lift Coefficient

The simulation results given in the foregoing sections demonstrate that the guidance system is capable of safely landing normal or impaired aircraft under widely varying operating conditions. The remaining investigations are those of guidance law robustness and near-optimality, discussed in the following sections.

E. Robustness Evaluation in Monte-Carlo Simulations

Since the closed-loop guidance law, together with the aircraft dynamics forms a nonlinear dynamic system, Monte Carlo simulation methodology can be used to assess the robustness of the system to parameter variations and disturbances.

All uncertainties except the wind gust and ground effect were assumed to be uniformly distributed random numbers. The following uncertainties are included in these simulations:

- Initial condition errors in altitude up to ±200 ft.
- Initial lateral offset from the runway up to ± 500ft.
- Initial heading angle errors of ± 5 degrees.
- Initial flight path deviations from the glideslope by ±0.15degrees.
- Loss of lift coefficient ranging between 35% and 45%.
- Random wind profiles were generated using the Dryden wind gust model. Figure 23 shows sample plots of wind components. The initial seed used in generating the band limited unit variance white noise signal is set to the Monte Carlo trial number.
- A Ground Effect model from Reference 20 is used in all the Monte Carlo simulation runs.

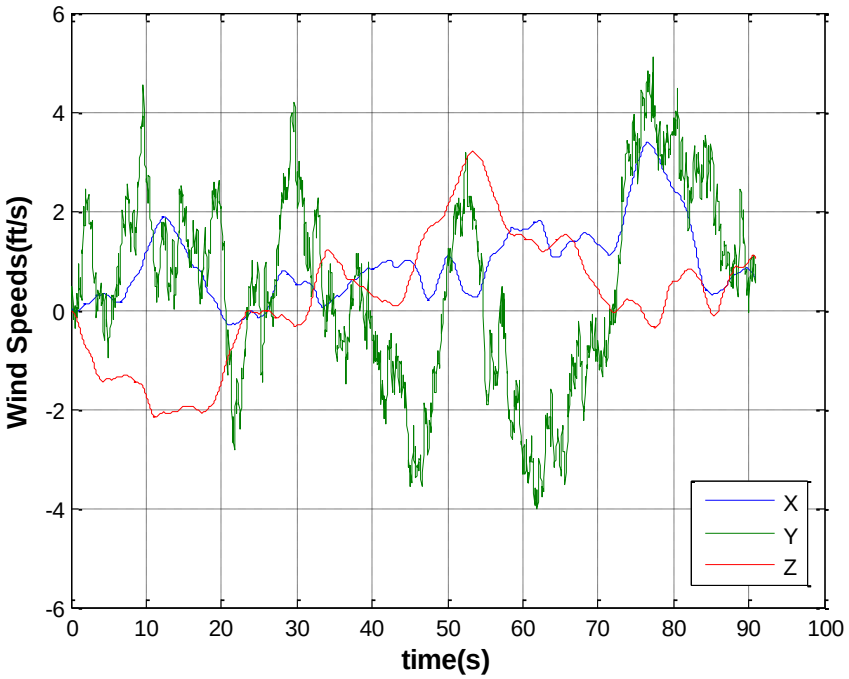

Figure 23. Wind Speeds from Dryden Wind Gust Model

The performance parameters of interest from the Monte-Carlo simulation trials are (i) descent rate at touchdown (ii) lateral offset at touchdown (iii) heading angle at touchdown and (iv) yaw attitude at touchdown. Figure 24 shows the distribution of the descent rates obtained from the 500 Monte Carlo simulation trials. The aircraft makes a positive touchdown (> 0ft/s descent rate) in 93% of the trials. The remaining 7% of the trials result in ballooning of the trajectory. It is noted that the descent rates at touchdown are lower than the intended 200 ft/min due to the extra lift derived from the ground effect model. The offset from the centerline at touchdown is less than 5 ft in all the trials as can be seen in Figure 25. The heading angle at touch is within ±1 degrees in most trials as seen in Figure 26. Finally, Figure 27 shows that the yaw attitude of the aircraft at touchdown is within ±0.05 degrees.

The Monte Carlo simulation results given in this section demonstrate that the guidance system is robust to system uncertainties and external disturbances within the specified uncertainty bounds. However, the present study needs to be significantly expanded with more realistic uncertainty bounds to gain further confidence in the robustness results.

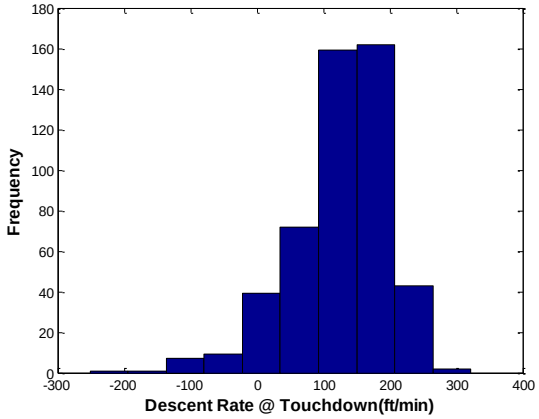

Figure 24. Distribution of Descent Rate at Touchdown

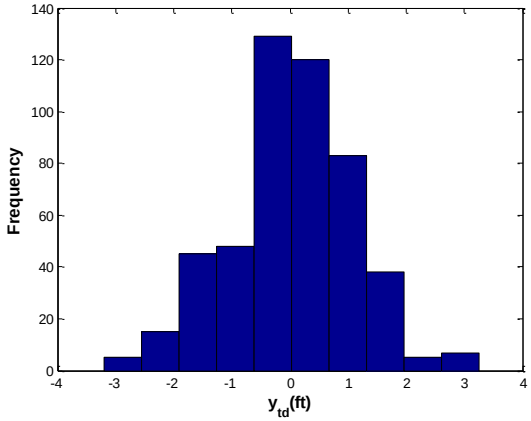

Figure 25. Distribution of Lateral Offset at Touchdown

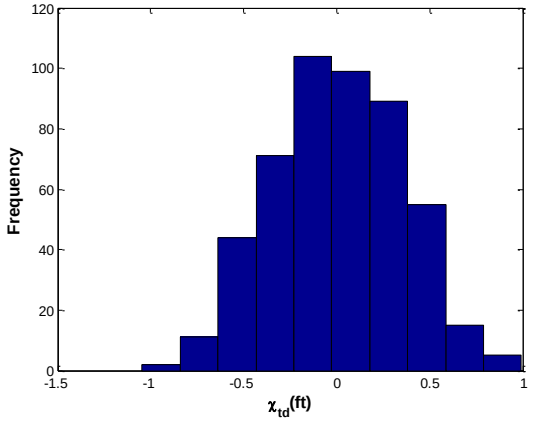

Figure 26. Distribution of Heading Angle at Touchdown

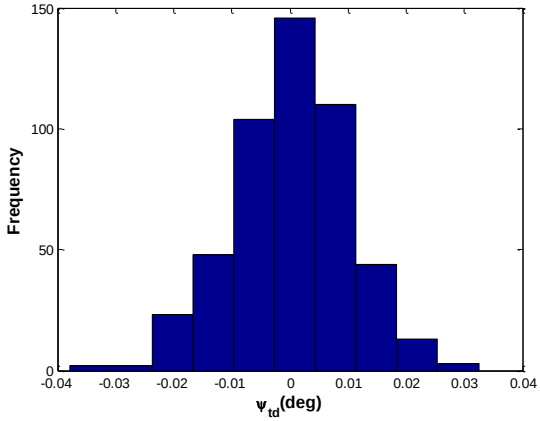

Figure 27. Distribution of Yaw Attitude at Touchdown

F. Near-Optimality of the Landing Guidance Law

In order to examine the near-optimality of the closed-loop guidance law based on transformed dynamics, a separate numerical trajectory optimization problem was formulated in the pitch plane. The performance index is chosen as the minimization of the integrated values of the load factor along the vertical plane trajectory. Note that the closed-loop guidance law formulation used the integral of the vehicle acceleration in the inertial frame. The desired boundary conditions are imposed as constraints in the problem. The pitch attitude history is approximated by piecewise quintic polynomials in time, in each of the three landing phases. The performance index is evaluated by simulating the vertical plane trajectory using the parameterized pitch attitude history. The coefficients of the polynomials describing the pitch attitude history were then chosen by a nonlinear programming algorithm. The MATLAB "fmincon[21]" is used in the present numerical optimization study. The optimization problem does not include the autopilot response to the guidance commands or the response of the engine to the thrust commands. Therefore, these dynamics are removed from the simulation model for the comparisons.

Trajectory and descent rates obtained from numerical optimization compare favorably with those obtained from closed-loop simulations as can be observed in Figure 28 - Figure 30. Both schemes achieve the desired waypoint conditions though the intermediate trajectories seem slightly different. Figure 31 and Figure 32 give the pitch attitude and the angle of attack histories. The plots are qualitatively similar in the stabilized approach segments, differing by less than a degree throughout the landing phase. The maximum angle of attack in the flare segment is

about 3.75 degrees and the maximum pitch attitude is 3 degrees, indicating very small flight path angle at the time of touchdown.

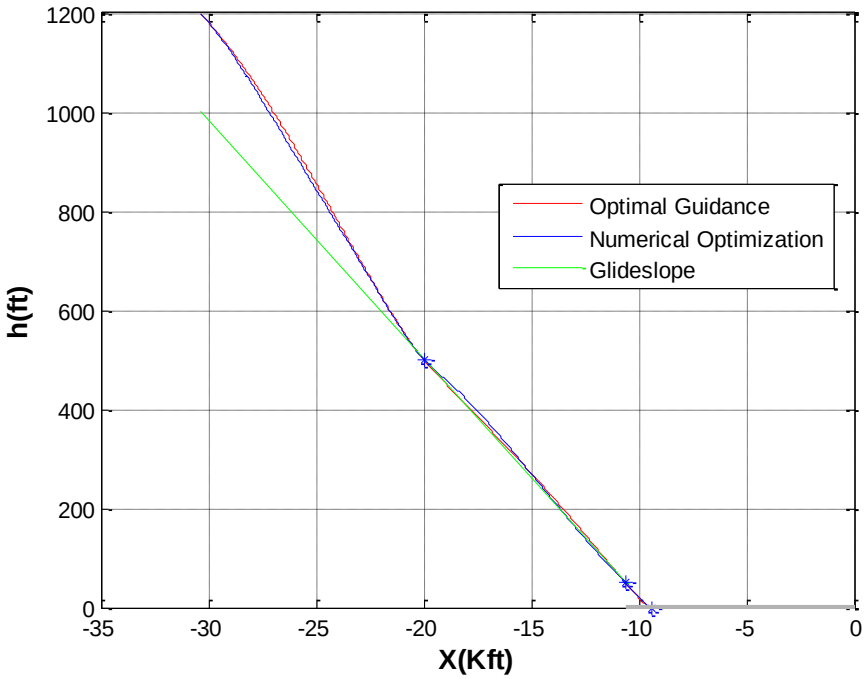

Figure 28. Comparison between Altitude Histories during Stabilized Approach and Flare

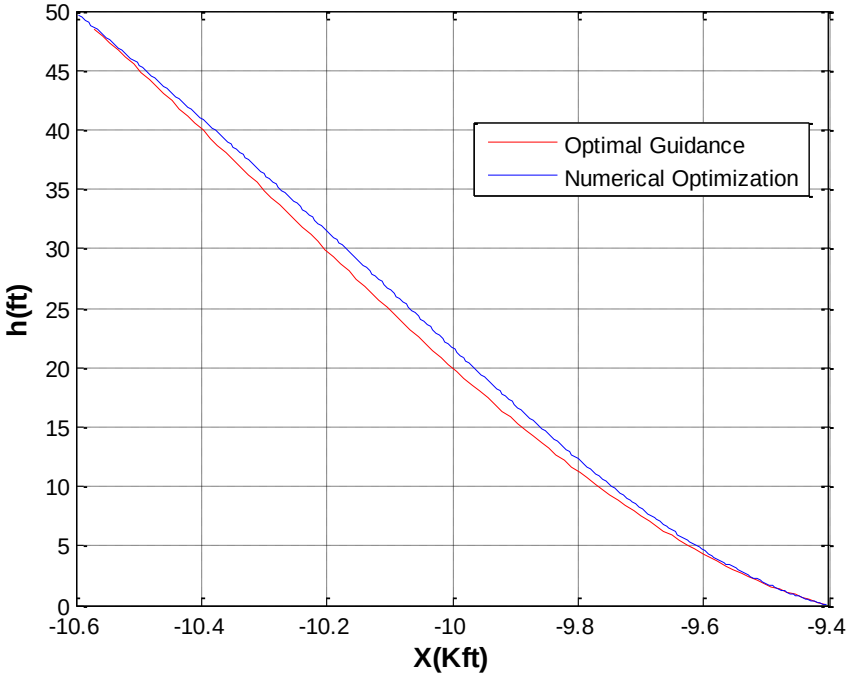

Figure 29. Comparison between Altitude Histories during the Flare Maneuver

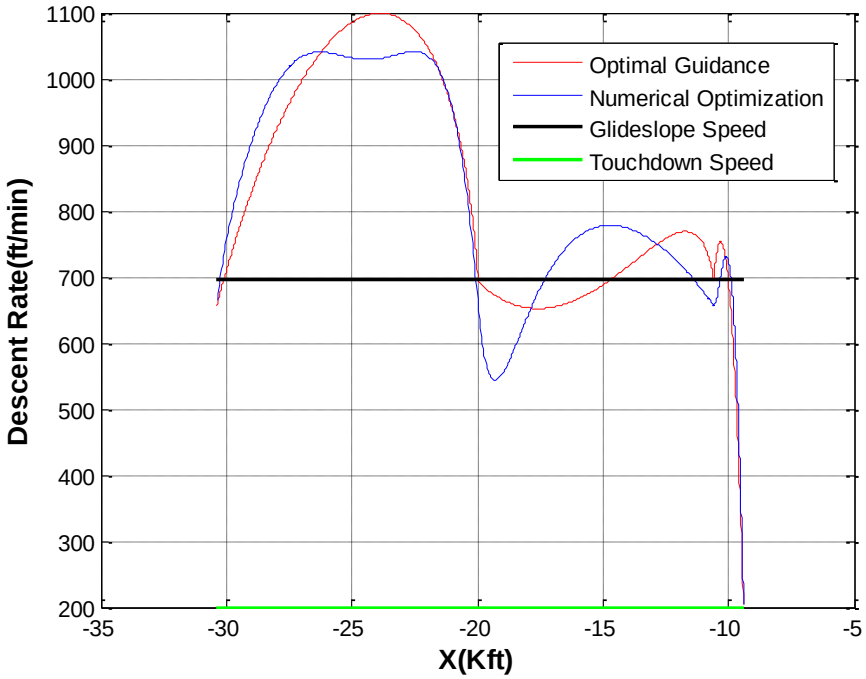

Figure 30. Comparison between Descent Rate during Stabilized Approach and Flare

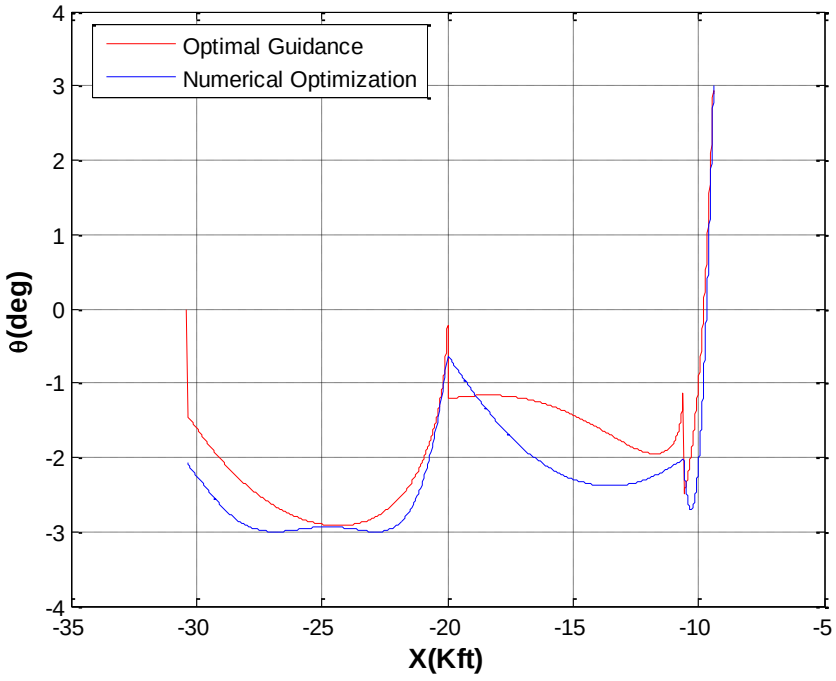

Figure 31. Comparison between Pitch Attitude Histories during the Stabilized Approach and Flare

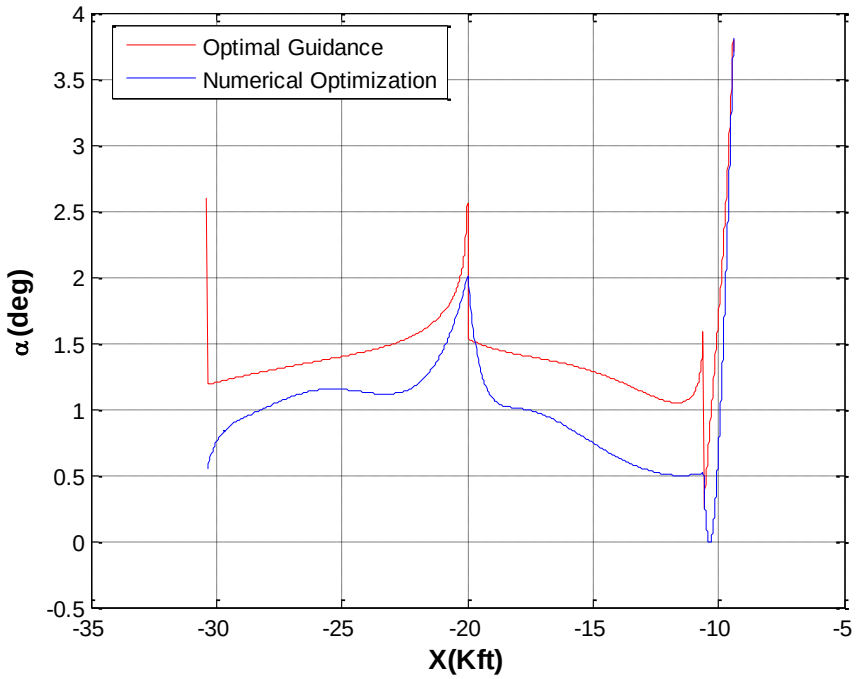

Figure 32. Comparison between Angle of Attack Histories during the Stabilized Approach and Flare

These numerical optimization results demonstrate the near-optimality of the closed-loop guidance law. Minor differences observed may be attributed to the differences in the performance index and the parameterization of the pitch attitude.

V. Conclusion

This paper described the development of a landing guidance law that can be used under normal and impaired conditions. Guidance law derivation employs feedback linearized nonlinear point-mass dynamic model of the aircraft. The system dynamics was transformed to a linear, time-invariant, decoupled form using differential geometric transformation. Differential game theory is then employed to synthesize the guidance law. Inverse transformation of the guidance law then produces a nonlinear, time-varying, coupled guidance law. Specialization of the guidance law for bank-to-turn and skid-to-turn maneuvers was illustrated. Performance of the guidance law under normal, as well as impaired aircraft conditions was then demonstrated. Robustness of the guidance law to a class of disturbances such as crosswind, wind gust, aerodynamic model uncertainties and ground effect was demonstrated in Monte Carlo simulations. Finally, the guidance law performance is compared with a numerically optimized trajectory to verify the near-optimality of the proposed approach. Evaluation of this guidance law in manned simulations will be of future interest.

Acknowledgments

This research was supported under NASA Contract number NNX09CC01P, with Mr. John Kaneshige as the Technical Monitor. The authors would like to thank Mr. Kaneshige, Dr. K. Krishnakumar and Dr. Nhan Nguyen of NASA Ames Research Center for their support and enthusiasm for this research. Ms. Vivian Lin of Optimal Synthesis Inc developed the data interface with FlightGear simulation program to create the animations used in evaluating the simulation results.

References

[1]Nguyen, N., Krishnakumar, K., Kaneshige, J., and Nespeca, P., "Dynamics and Adaptive Control for Stability Recovery of Damaged Asymmetric Aircraft," *AIAA Guidance, Navigation, and Control Conference,* August 21- 24, 2006, Keystone, CO., Paper # AIAA 2006-6049.

[2]Nguyen, N., Krishnakumar, K., Kaneshige, J., and Nespeca, P., "Flight Dynamics and Hybrid Adaptive Control of Damaged Aircraft," *Journal of Guidance, Control, and Dynamics*, Vol. 31, No. 3, May-June 2008.

[3]Rysdyk, R. T., and Calise, A. J., "Fault Tolerant Flight Control via Adaptive Neural Network Augmentation," *1998 AIAA Guidance, Navigation, and Control Conference*, Paper No. AIAA-1998-4483.

[4]Anon, *Airplane Flying Handbook*, Document No. FAA-H-8083-3A, U.S. Department of Transportation – Federal Aviation Administration, Washington, D. C., 2004.

[5]Kim, J., Palaniappan, K. and Menon, P. K., "Rapid Estimation of Impaired Aircraft Aerodynamic Parameters Aircraft Performance Models using Differential Vortex Panel Method and Extended Kalman Filter," to appear in the *Journal of Aircraft*, 2010.

[6]Anon, *Code of Federal Regulations- Part 14, Aeronautics and Space, Parts 1 to 50*, U. S. Government Printing Office, Washington, DC, January 1, 2007.

[7]http://www.youtube.com/, July 14, 2010.

[8]McLean, D., *Automatic Flight Control Systems*, Prentice Hall, New York, NY, 1990.

[9]McRuer, D., Ashkenas, I., and Graham, D., *Aircraft Flight Dynamics and Automatic Control*, Princeton University Press, Princeton, NJ, 1973.

[10]Jorgensen, C. C., and Schley, C., "A Neural Network Baseline Problem for Control of Aircraft Flare and Touchdown," in *Neural Networks for Control*, Edited by: W. T. Miller III, R. S. Sutton and P. J. Werbos, The MIT Press, Cambridge, MA 1990.

[11]Bryson, A. E., and Ho, Y. C., *Applied Optimal Control*, Hemisphere, New York, NY, 1975.

[12]Issacs, R., *Differential Games*, Robert E. Krieger Publishing Company, Huntington, NY, 1975.

[13]Menon, P. K., "Short-Range Nonlinear Feedback Strategies for Aircraft Pursuit-Evasion," *Journal of Guidance, Control and Dynamics*, Vol. 12, January - February 1989, pp. 27 - 32.

[14]Menon, P. K., and Duke, E. L., "Time-Optimal Aircraft Pursuit-Evasion with a Weapon Envelope Constraint," *Journal of Guidance, Control, and Dynamics*, Vol. 15, No. 2, March - April 1992, pp. 448-456.

[15]Menon, P. K. and Calise, A. J., "Interception, Evasion, Rendezvous, and Velocity-to-be-Gained Guidance for Spacecraft," *AIAA Guidance, Navigation and Control Conference*, August 17-19, 1987, Monterey, CA.

[16]Menon, P. K., "Aerobrake Guidance Law Synthesis Using Feedback Linearization," *1991 American Control Conference*, June 26-28, Boston, MA.

[17]Kreyszig, E., *Differential Geometry*, Dover, New York, NY, 1991

[18]Isidori, A., *Nonlinear Control Systems*, Springer-Verlag, New York, NY, 1985

[19]Marino, R., Tomei, P., *Nonlinear Control Design*, Prentice Hall, New York, NY, 1995.

[20]"FLTz Aircraft Simulation Software Version 4.2", NASA Technical Point of Contact : John Kaneshige, Code TI, NASA Ames Research Center, Mail Stop: 269-1, Moffet Field, CA, 94035-1000, Feb 2009.

[21]Anon, *Optimization Toolbox for MATLAB®*, The MathWorks, Inc., Natick, MA, 2007.